Electronic Supplementary Material (ESI) for Journal of Materials Chemistry C.

Supporting Information

Experimental and theoretical evidence for temperature driving electric-magnetic complementary effect in magnetic microwave absorbing materials

Xuan Yang, Yuping Duan, Yuansong Zeng, Huifang Pang*, Guojia Ma, Xuhao Dai*

Supporting Figures

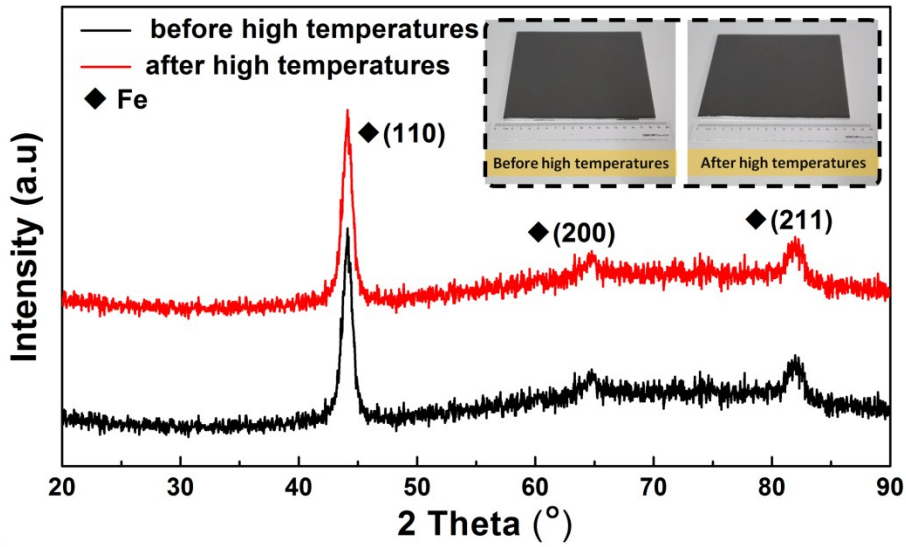

Supporting Figure 1 XRD pattern of coating before and after high temperatures. The coating surface was smooth and dense without significant change before and after high temperatures. The diffraction patterns of coating have little change before and after high temperatures. The characteristic peaks appear at 44.35°, 64.52° and 81.65°, which are assigned to (110), (200) and (211) crystal planes of iron respectively. These similar diffraction patterns indicates that there is no oxidation of CIPs during the high temperatures test.

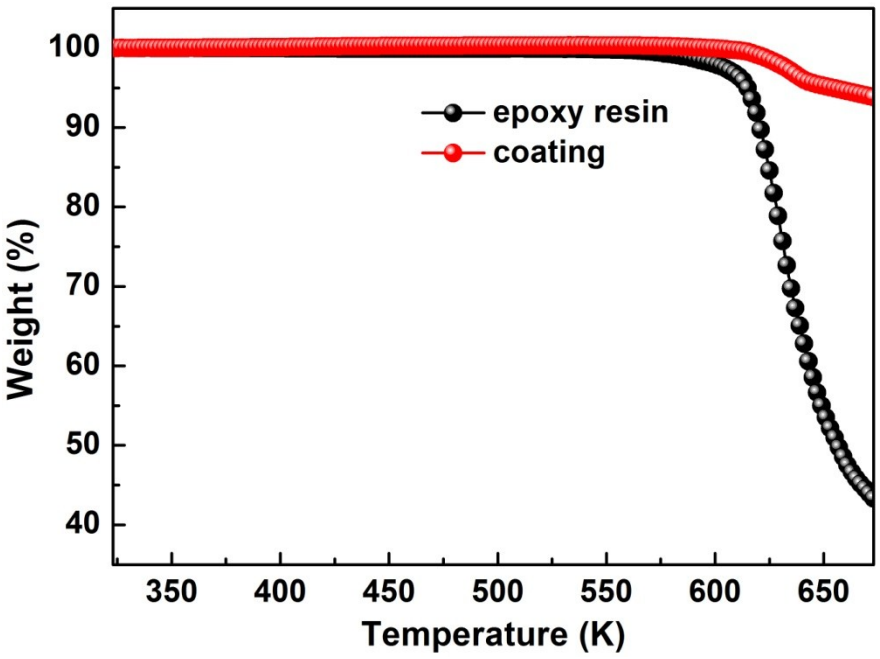

Supporting Figure 2 TGA analysis of epoxy resin and coating.

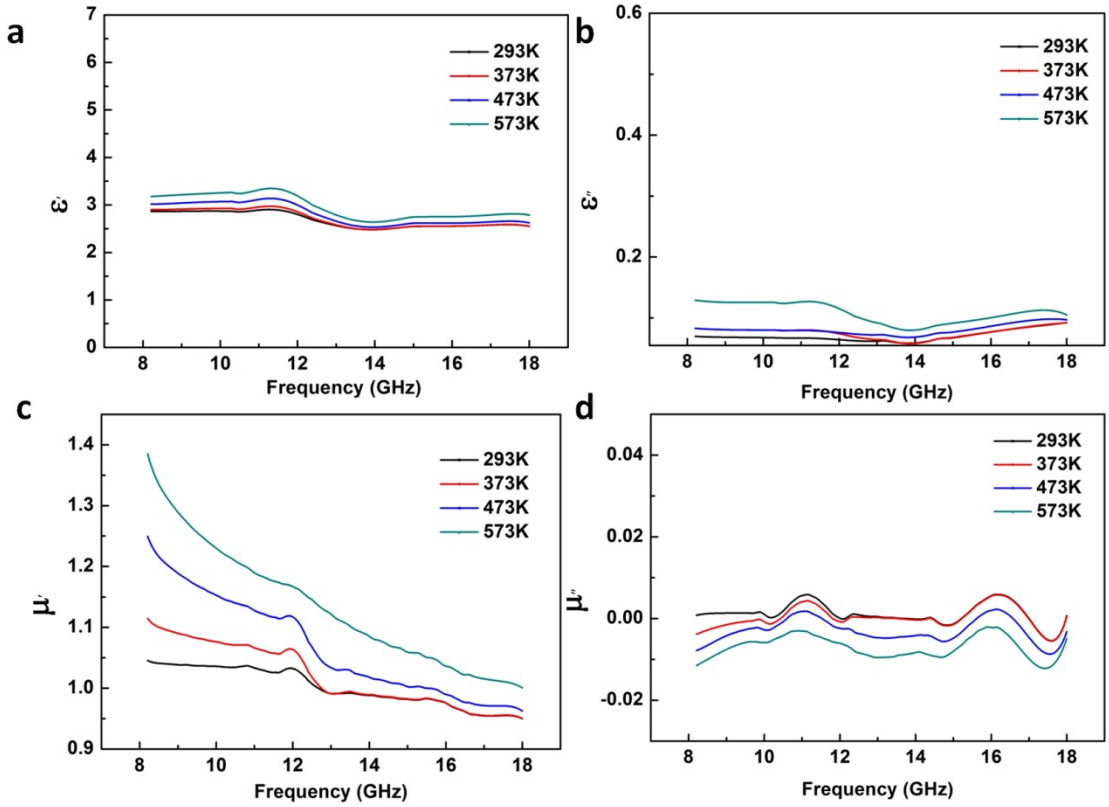

Supporting Figure 3 Frequency dependence of electromagnetic parameters of epoxy resin at different temperatures. (a) The real part of complex permittivity. (b) The imaginary part of complex

permittivity. (c) The real part of complex permeability. (d) The imaginary part of complex permeability.

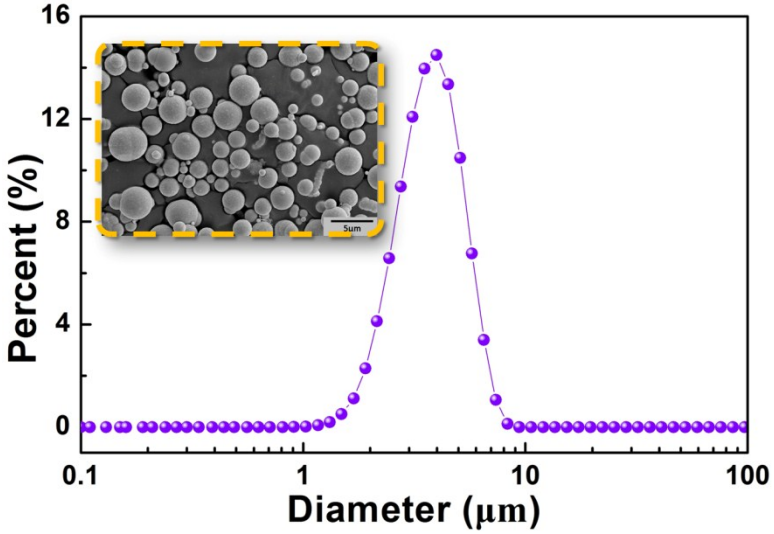

Supporting Figure 4 Size distribution of CIPs. The particle size test results are consistent with the observations of SEM, and the CIPs size distribution is relatively concentrated from 0.91 μm to 8.32 μm.

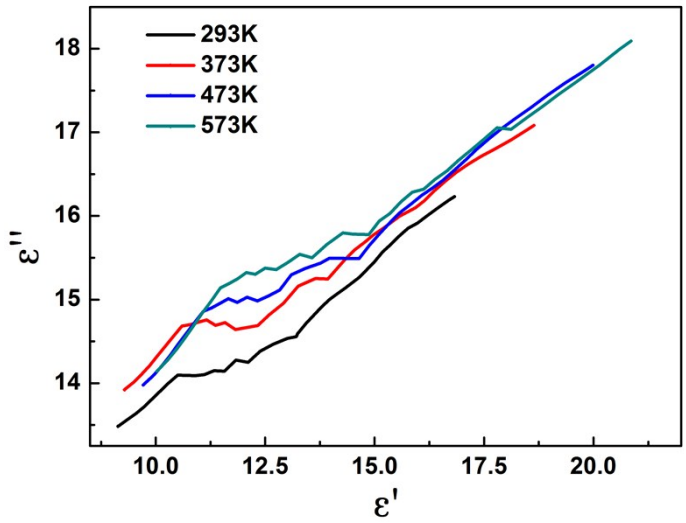

Supporting Figure 5 Cole-Cole plots at different temperatures. C-C semicircles are the important symbols of polarization relaxation, and one semicircle represents one pattern of polarization relaxation. If the plot is close to a straight line, the polarization relaxation is very weak in this system. Therefore, these plots are close to straight lines at different temperatures indicate that the polarization relaxation loss can be ignored in the coating.

Supporting Equations

$$\mu_i - 1 = \frac{4\pi}{\frac{H_k}{M_s} + 4\pi N_h} \tag{1}$$

where H_k is the magnetocrystalline anisotropy field; N_h is the demagnetization factor; M_s is the saturation magnetization of CIPs. In our case, due to the use of spherical CIPs, there is no significant anisotropy, and the particle size as well as crystal structure do not change obviously during the entire heating process. Hence, H_k and N_h are not the main factor causing the change in μ_i.

$$f = 2\pi\omega \tag{2}$$

$$\frac{\omega}{\gamma} = \frac{Q\mu_{kn}^2}{r^2 M_s} + H \tag{3}$$

$$H = H_0 - \frac{4\pi M_s}{3} + \frac{2k}{M_s} = H_0 - \frac{2M_s}{3}(2\pi - \frac{\mu_0}{\mu_i}) \tag{4}$$

where f is the frequency, ω is angular frequency, γ is gyromagnetic ratio, Q is exchange constant, H is magnetic field, μ_{kn} is root of spherical Bessel function, r is particle size, μ_i is initial susceptibility, μ_0 is vacuum permeability, and H_0 is applied field. In the above three formulas, all parameters except M_s, ω, f, μ_i and H are constant.

Therefore, there is a corresponding relationship between M_s and exchange resonance frequency.[1]

$$C_0 = \mu''(\mu')^{-2} f^{-1} = \frac{2\pi\sigma\mu_0 d^2}{3} \quad (5)$$

where C_0 is the eddy current coefficient, σ is the conductivity, d is thickness of the region that generates the eddy current. The parameters on the right side of the Supplementary Equation 5 are constant at the same temperature, so C_0 is constant when there is only eddy current loss.[2]

$$\varepsilon'(T) = \varepsilon_\infty + \frac{\varepsilon_s - \varepsilon_\infty}{1 + \omega^2 \tau(T)^2} \quad (6)$$

$$\tau(T) = \tau_0 e^{\frac{E_d}{RT}} \quad (7)$$

where $\tau(T)$, ε_s, ε_∞, ω, T, τ_0 and E_d are the temperature-dependent relaxation time, static dielectric constant, dielectric constant at infinite frequency, angular frequency, temperature, prefactor and activation energy, respectively.

Supporting Note 1: Simulation of conductivity and current density distribution at MIM junction

Due to the curing nature of epoxy resin, it is difficult to prepare cross-sectional samples for the precise characterization of the metal-insulator-metal junctions thickness using transmission electron microscopy. However, it can be estimated theoretically via the numerical calculations. In general, the insulating barrier layer in the MIM junction is modeled as rectangular barrier or trapezoidal barrier.[3] For our case, the fluctuating voltage generated by the temperature change causes a barrier height difference across the insulating layer, so the insulating barrier layer is more suitable for modeling into the trapezoidal barrier. Based on the one-dimensional trapezoidal tunnel barrier model (Figure 5e), we define that electrons with mass m and energy E are projected to the trapezoidal barrier along the positive x-axis. The barrier function of trapezoidal barrier can be expressed by following equation:

$$U(x) = U_0 - \frac{x}{d}V_T \tag{8}$$

where U_0 is the initial barrier height, d is the tunneling spacing between two CIPs, V_T is the fluctuating voltage. When a large number of electrons are incident into a trapezoidal barrier, only electrons

whose wave function satisfies the corresponding stationary Schrödinger equation ψ can complete tunneling and other electrons will be reflected to other directions. Here, the Wentzel-Kramers-Brillouin (WKB) approximation method[4] is used to solve ψ, as follows:

$$\begin{cases} \dfrac{d^2\psi}{dx^2} + \dfrac{2m}{\hbar^2}E\psi = 0 & x < 0, x > d \\ \dfrac{d^2\psi}{dx^2} + \dfrac{2m}{\hbar^2}[E - U(x)]\psi = 0 & 0 < x < d \end{cases} \tag{9}$$

where $\hbar$ is the Planck constant. We pay more attention to the tunneling coefficient t throughout the solution process, which indicates the probability of electrons completing tunneling. Specifically, depending on the electrons energy and average height of barrier, the calculation of t can be divided into the following three parts.[5]

$$\begin{cases} t = \dfrac{4K_1^2\bar{K}_2{}^2}{(K_1^2 - \bar{K}_2{}^2)^2 \sin^2 d\bar{K}_2 + 4K_1^2\bar{K}_2{}^2} & E > \bar{U} \\ t = \dfrac{1}{1 + 0.25d^2K_1^2} & E = \bar{U} \\ t = \dfrac{4K_1^2\bar{K}_3{}^2}{(K_1^2 - \bar{K}_3{}^2)^2 \mathrm{sh}^2\, \mathrm{d}\bar{K}_2 + 4K_1^2\bar{K}_3{}^2} & E < \bar{U} \end{cases} \tag{10}$$

$$\begin{cases} \bar{U} = \dfrac{\int_0^d U(x)dx}{d} \\ K_1 = \left[\dfrac{2mE}{\hbar^2}\right]^{\frac{1}{2}} \\ \bar{K}_2 = \dfrac{\int_0^d \sqrt{2m[U(x) - E]}dx}{\hbar d} \\ \bar{K}_2 = i\bar{K}_3 \end{cases} \tag{11}$$

In our case, the change in temperature not only affects the magnitude of fluctuating voltage, but also affects the energy distribution of electrons. Therefore, combining these two aspects, the tunneling current, $I(V_T)$, at different temperatures can be described by the following equation:

$$I(V_T) = \frac{2\pi e}{h}\int_0^{E_f} t(E,V_T)\left[f(E) - f(E+V_T)\right]d \tag{12}$$

where E_f is the Fermi level, h is the reduced Planck constant, e is the elementary charge (1.6×10^{-19} C). Moreover, $f(E)$ is the Fermi-Dirac distribution described by equation (13):

$$f(E) = \left\{1 + exp\left[\frac{(E - E_f)}{Tk_B}\right]\right\}^{-1} \tag{13}$$

where k_B is the Boltzmann constant (1.38×10^{-23} J/K). On the other hand, due to the randomness of the thermal motion of electrons, the probability of voltage fluctuations is another key factor affecting the conductivity of MIM junctions. Hence, the probability of voltage fluctuations at different temperatures should be included in the calculation to further improve the accuracy. The specific calculation formula is as follows:

$$P(V_T) = (\frac{2C}{\pi T k_B})^{\frac{1}{2}} exp(-\frac{C}{2Tk_B}V_T^2) \tag{14}$$

where C represents the equivalent capacitor with area S(0.5×10^{-18}m^2). Based on the above derivation, the conductivity expressions (Supplementary Equation 15) of MIM junctions controlled by tunneling effect at different temperatures and corresponding current density distribution (Supplementary Equation 16) can be obtained.

$$\sigma = \int_0^{\infty} P(V_T)\frac{dI(V_T)}{dV_T}dV_T \tag{15}$$

$$j = \frac{I(V_T)}{S} \tag{16}$$

In the calculation of the tunneling current through the MIM junctions, the thickness of the insulating layer is adjusted and the

correct value is ascertained by matching the magnitude of the calculated conductivity curve to the experimentally measured one. The thickness of the insulating layer is found to be ~4.67 nm.

Supporting Note 2: Calculation of conductivity generated by thermal electron emission at MIM junction

It is possible for electrons with energy exceeding the barrier to complete electron emission and the electron energy distribution is closely related to the temperature. Therefore, the temperature has an important influence on the thermal electron current. The current density generated by thermal electron emission at different temperatures can be calculated by following Richardson Dushman equation:[6]

$$I_0 = AT^2 e^{\left(-\frac{\phi}{kT}\right)} \tag{17}$$

where I_0 is the zero-field emission density, T is the temperature, A is the emission constant (120 $Acm^{-2}K^{-2}$), k is the Boltzmann constant (8.62×10^{-5} eV/K), ϕ is the work function (4.5 eV for iron). The calculation results are shown in Table 1, and it is clear that the current density generated by thermionic emission is significantly less than that of tunneling effect. For CIPs at the temperature range of 293 K-573 K, although the increase in temperature enhances the energy of electrons, only a very small amount of electrons have higher energy than barrier, completing thermal electron emission. By contrast, the

energy of electrons participating in the tunneling effect is not necessarily exceeding the barrier, and an increase in temperature can effectively boosts the fluctuation voltage to adjust barrier shape, further improving the probability of tunneling effect. Therefore, tunneling effect is the main mechanism for controlling electrons transfer in temperature range 293 K- 573 K.

Table 1 Current density of thermal electron emission for MIM junctions at different temperatures.

Temperature (K)	293 K	373 K	473 K	573 K
Current density (A/cm^2)	1.47×10^{-73} A/cm^2	7.38×10^{-57} A/cm^2	6.63×10^{-44} A/cm^2	1.86×10^{-35} A/cm^2

References

[1] a) J. Ramprecht, D. Sjöberg, *Journal of Physics D: Applied Physics* **2008**, 41, 135005; b) F. Wen, H. Yi, L. Qiao, H. Zheng, D. Zhou, F. Li, *Applied Physics Letters* **2008**, 92, 1032.

[2] P. Yang, Y. Liu, X. Zhao, J. Cheng, H. Li, *Advanced Powder Technology* **2016**, 27, 1128.

[3] P. Wang, A. V. Krasavin, M. E. Nasir, W. Dickson, A. V. Zayats, *Nature Nanotechnology* **2018**, 13, 159.

[4] a) J. W. Conley, C. B. Duke, G. D. Mahan, J. J. Tiemann, *Physical Review* **1968**, 150, 466; b) N. Jalili, *Piezoelectric-Based Micro- and Nano-Positioning Systems*, **2010**.

[5] E. Burstein, S. Lundqvist, *Tunneling Phenomena in Solids*, **1969**.

[6] a) A. L. Smith, R. Breitwieser, *Journal of Applied Physics* **1970**, 41, 436; b) S. Elfimchev, M. Chandran, R. Akhvlediani, A. Hoffman, *Applied Surface Science* **2017**, 410, 414.